ACS NANO
Cite This: ACS Nano XXXX, XXX, XXX−XXX
www.acsnano.org

ARTICLE

Fiber-Coupled Luminescent Concentrators for Medical Diagnostics, Agriculture, and Telecommunications

Nikolay S. Makarov,* Karthik Ramasamy, Aaron Jackson, Andres Velarde, Chloe Castaneda, Nic Archuleta, Damon Hebert, Matthew R. Bergren, and Hunter McDaniel

UbiQD, Inc., Los Alamos, New Mexico 87544, United States

Supporting Information

ABSTRACT: While luminescent concentrators (LCs) are mainly designed to harvest sunlight and convert its energy into electricity, the same concept can be advantageous in alternative applications. Examples of such applications are demonstrated here by coupling the edge-guided light of high-performance LCs based on $CuInSe_xS_{2-x}$/ZnS quantum dots into optical fibers with emission covering visible-to-NIR spectral regions. In particular, a cost-efficient, miniature broadband light source for medical diagnostics, a spectral-conversion and light-guiding device for agriculture, and a large-area broadband tunable detector for telecommunications are demonstrated. Various design considerations and performance optimization approaches are discussed and summarized. Prototypes of the devices are manufactured and tested. Individual elements of the broadband light source show coupling efficiencies up to 1%, which is sufficient to saturate typical fiber-coupled spectrometers at a minimal integration time of 1 ms using 100 mW blue excitation. Agricultural devices are capable of delivering ∼10% of photosynthetically active radiation (per device) converted from absorbed sunlight to the lower canopy of plants, which boosted the tomato yield in a commercial greenhouse by 7% (fresh weight). Finally, large-scale prototype detectors can be used to discern time-modulated unfocused signals with an average power as low as 1 μW, which would be useful for free-space telecommunication systems. Fully optimized devices are expected to make significant impacts on speed and bandwidth of free-space telecommunication systems, medical diagnostics, and greenhouse crop yields.

KEYWORDS: *fiber-coupled luminescent concentrator, quantum dot, spectral tissue sensing, lower canopy lighting, large area luminescent detector*

Since the introduction of the luminescent concentrators (LCs) in the mid-1970s,[1] the technology has mostly been developed for use as large-area (>1 m^2) solar energy collectors in windows.[2−5] Therefore, a traditional LC is a large-area device consisting of a transparent surface (glass or plastic) with incorporated emissive chromophores such as organic dyes, rare-earth elements, or quantum dots (QDs). In an LC, incident light is first absorbed by chromophores and then re-emitted at a longer wavelength and waveguided to the edges of the LC by total internal reflection. Generally, solar cells are attached along the perimeter of the LC to absorb the waveguided light and generate electricity. The application best suited for this type of device is generating electricity from transparent surfaces, such as windows or curtain walls, which generally have a large area (>1 m^2). However, there are other applications which can make use of smaller devices, which are typically more efficient than their large-area counterparts.[6] As described below, these applications include medical devices, agriculture optimization, and telecommunications.

According to the American Cancer Society, the largest economic losses for the United States can be attributed to cancer. The disease costs the country >1.7% of its GDP, with more than 1.6 M new cancer cases diagnosed annually.[7] Of those diagnosed, more than 600,000 people die from the disease every year.[7] Early diagnosis of cancer greatly improves an individual's chance for survival because current cancer treatments are more effective during the early stages of the disease.[8] Furthermore, the accuracy of treatment can greatly reduce the risks of recurrence and metastasis. Spectral tissue sensing (STS) is seen as a promising tool for early and accurate cancer detection. STS works by determining the optical properties of tissues, which can be correlated to healthy and cancerous tissues. To date, STS is being investigated as an aid for detecting cancers,[9−12] monitoring morphological and

Received: April 30, 2019
Accepted: July 10, 2019
Published: July 10, 2019

DOI: 10.1021/acsnano.9b03335
ACS Nano XXXX, XXX, XXX−XXX

physiological changes of tissue,[13] and monitoring therapy response, for instance, in photodynamic therapy.[14] Multiple clinical studies have shown that by analyzing the information on intrinsic physiological tissue properties, such as oxy- and deoxy-hemoglobin, water, and lipids content obtained by STS, one can successfully diagnose breast cancer with sensitivity and specificity as high as 100% and 96%, respectively.[10−12,15−18] STS utilizes absorption and scattering of broadband light, up to wavelengths ∼1600 nm, to analyze the concentration of oxy- and deoxy-hemoglobin (visible light), as well as water and lipids, which have distinct absorption peaks in the near-infrared (NIR) spectral region.[19] However, it has been difficult to realize a low-cost miniature commercial diagnostic system due to inadequate broadband illumination sources. Until recently, the only appropriate broadband light source was a fiber-coupled tungsten halogen bulb. Recently, however (Feb 2019), Lumileds announced Luxion IR Onyx light emitting diode (LED) for use in medical applications, which has a flat emission in the wavelengths range between 650 and 1100 nm. Still, this product lacks fiber-coupling and offers limited spectral range.

Various teams have worked on developing integrated spectrometers for STS. One of the major challenges for such a device is illuminating a sample with a continuous spectrum covering the visible and NIR spectral regions. To do so, one has to rely on bulky and inefficient lamps that are too weak to achieve a sufficient signal-to-noise ratio. Thus, a miniature, bright, and low-cost fiber-coupled illumination source is highly desired. One potential device design is to down-convert a blue or ultraviolet (UV) LED excitation into a broadband spectrum using multiple phosphor materials with different emission peaks. Important requirements for such phosphor materials include broad emission of individual species (to minimize the number of phosphor materials), low reabsorption (for efficient light-guiding), high quantum yield (QY, to increase overall efficiency), strong absorption at the excitation wavelength, and small (nm-scale) physical size to minimize scattering losses. The materials should also be non-toxic for clinician and patient safety but also for a more environmentally sustainable waste stream.

$CuInSe_xS_{2-x}$/ZnS QDs are attractive luminophore candidates for STS because they possess all of the desired properties (Table 1, Supporting Information). In particular, $CuInSe_xS_{2-x}$/ZnS QDs maintain high photoluminescence (PL) QY across a broad spectral range covering visible-to-NIR, show minimal reabsorption due to an inherently large Stokes shift, and their few-nanometer size scale is much smaller than the emitted wavelengths. Here we describe a promising broadband light source design consisting of a group of fiber-coupled LCs (FC-LCs), where each fiber individually emits a portion of a broadband spectrum. The fiber's individual outputs are then bundled in a single optical fiber used for medical diagnostics.

The broadband light source is not the only application to benefit from the use of FC-LCs. Other applications, such as agriculture, can also benefit from the use of this technology. It is commonly known that photosynthetically active radiation (PAR)—light with wavelengths between 400 and 700 nm—is the most useful for supporting plant growth. Photosynthetic photon flux (PPF) is the typical metric used by growers to gauge the number of PAR photons incident upon an area per unit time.[20] One way to improve plant growth is to provide more PAR light to leaves located below the top of the plant (lower canopy, so-called intercanopy lighting), which ultimately improves photosynthetic production in the plant and increases the plant yield. The leaves of a mature plant, for example, do not get the same average amount of sunlight. In fact, the leaves in the lower canopy of the plant are typically getting 1/10th of light compared to the leaves in the top canopy. There exist numerous commercially available artificial lighting systems that provide intercanopy lighting; however, these solutions are typically expensive at ∼\$50/ft^2 and significantly increase electricity costs for plant growers. Additionally, they introduce excess heat into the growth environment, thus adding cooling and humidification costs in some climates. Therefore, it is beneficial to design a passive device that can effectively harvest some of the sun's spectrum, modify it, and guide the light to the lower canopy of the plants. The quality of spectrum also has to be considered for lower canopy lighting, as different wavelengths of light are more efficient for photosynthesis than others, within the PAR spectrum.[21−24] Thus, the purpose of the FC-LC-based waveguiding light collector described here is 2-fold: to increase the number of PAR photons absorbed by the plants and to provide an optimum spectrum for efficient and improved plant growth. Similar to medical FC-LCs, $CuInSe_xS_{2-x}$/ZnS QDs are a promising choice as an active material for FC-LCs used for intercanopy lighting.

Another area that can benefit from small-scale FC-LCs is in free-space telecommunications. High demand for fast-data-rate wireless communication motivates alternative approaches based on various optical schemes. Trade-offs in electronics constrain the speed, size, and sensitivity of semiconductor photodiodes, which are commonly used as detectors in optical communication. For example, since the response time of a detector is linked to its physical size, achieving fast speeds (bandwidth on the order of GHz) requires detectors with an active area on the order of 1 mm^2—much smaller than the typical size of the laser beams used in free-space optical telecommunication after the light travels a large distance through the atmosphere. To avoid this size mismatch, one can focus the light on the detectors using active tracking systems which can compensate for the pointing instability of light due to atmospheric effects. However, this makes telecommunication systems significantly more complicated and, thus, increases their cost and reduces reliability. As a potential solution to avoid complex optics, large-area luminescent detectors have been proposed.[25]

Relatively large-area (cm^2 sizes compared to current mm^2 detector sizes) LC-based receivers can mitigate the complexity of such telecommunication systems by allowing a larger active size and a larger field of view of the detectors while preserving the fast speed of small photodiodes. Essentially, this is achieved by separating light detection into two independent parts: collection of the light transmitted through large distance and thus affected by pointing instability is achieved optically by LC and the transformation of the photons into electrons is achieved by a small-area fast photodetector. In this case, the active area of the detection system can be increased by up to 3 orders of magnitude without sacrificing the bandwidth of the detection system.[25] While the working principles of these devices have been demonstrated previously, and multi-Gbps data rates with standard modulation schemes and excitation peak intensities of ∼1 mW/cm^2 have been reported,[25] the use of commercially available luminescent materials in large-area detector applications remains far from optimized. Once again $CuInSe_xS_{2-x}$/ZnS QDs, which combine the benefits of strong

DOI: 10.1021/acsnano.9b03335
ACS Nano XXXX, XXX, XXX−XXX

Scheme 1. Design Possibilities for a Fiber-Coupled Broadband Light Source[a]

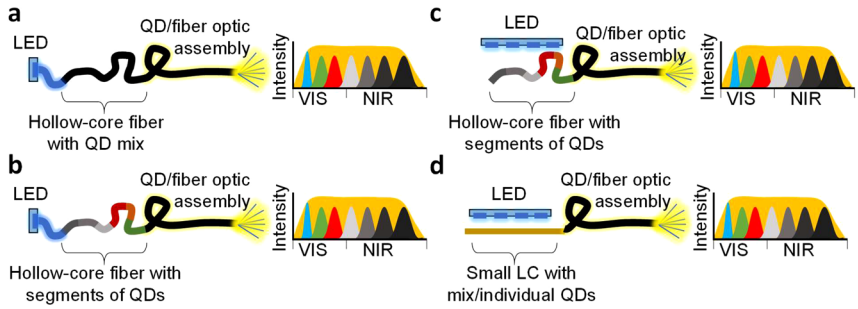

[a]Key: (a) In its simplest implementation, QDs (or other phosphors) are incorporated in an optical fiber next to the fiber-coupled LED. (b) In order to mitigate reabsorption issues, QDs are separated into different fiber segments with the furthest NIR-emitting QDs closer to the excitation and the most blue-emitting QDs further from the excitation. This way, reabsorption of the visible emission by NIR QDs is eliminated. (c) In order to reduce cost of the device, a free-space LED is used instead of the fiber-coupled LED. (d) In order to maximize efficiency of the free-space LED excitation, QDs are incorporated into small FC-LCs instead of optical fibers themselves.

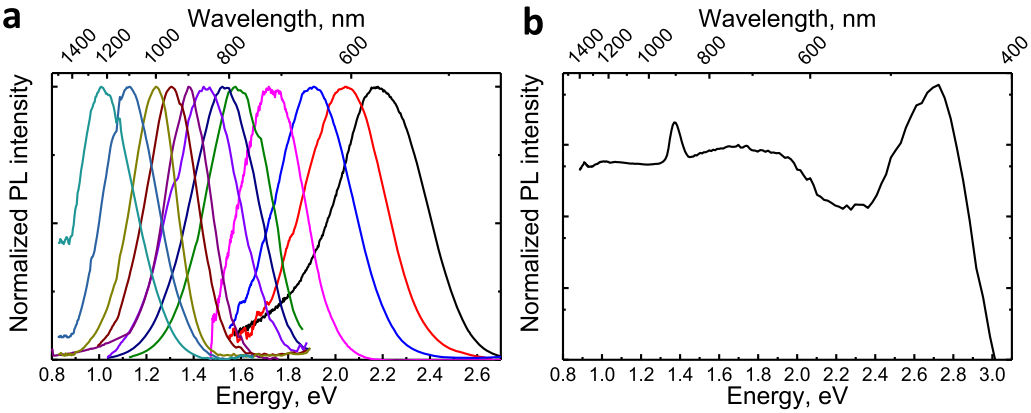

Figure 1. (a) PL spectra of the $CuInSe_xS_{2-x}$/ZnS QDs of varying sizes and compositions cover the spectral range from 550 to 1250 nm (peak positions). (b) Combining QDs emitting at 650, 780, 990, and 1150 nm in a polymer slab allows for broadband emission covering the 440−1400 nm spectral range when excited by a 450 nm LED. The spike at 900 nm is a second order of the excitation.

absorption, low reabsorption losses, high QYs, and easy processability, can serve as a promising tunable luminescent material for the large-area detectors.

In this paper, we first demonstrate that the $CuInSe_xS_{2-x}$/ZnS QDs incorporated in small FC-LCs are efficient as the basis of a broadband light source for medical diagnostics. Next, we show that a similar design can be used to transform the solar spectrum and improve the growth of plants in greenhouses. Finally, we demonstrate that the same concept of the FC-LC can be used to build efficient large-area receivers for free-space telecommunication.

RESULTS AND DISCUSSION

Fiber-Coupled Broadband Light Source for Medical Diagnostics. One of the major challenges for the design of a miniature fiber-coupled light source is overcoming the need for bulky reflectors and other focusing optics to maximize coupling efficiency. One way to simplify such a system is to use down-converting materials, coupled with LED excitation, which are directly incorporated into optical fibers (Scheme 1a). In this case, blue or UV light can be used to excite various phosphors contained within a fiber-optics package to emit a broadband spectrum. However, a mixture of phosphors with such broadband emission typically faces the problem of reabsorption. Namely, the emission from visible phosphors will be (partially) reabsorbed by phosphors emitting in the NIR spectral range, thus reducing device efficiency. By separating the phosphors into different segments along the length of the optical fiber, with NIR emitters closer to the excitation and visible emitters further away from the excitation (Scheme 1b), one can mitigate reabsorption in phosphor materials with large Stokes shifts. However, this reduced reabsorption comes at the price of increased device complexity and manufacturing cost. Additionally, both designs shown in Scheme 1a,b use moderately expensive fiber-coupled LEDs as the excitation source, while less expensive free-space LEDs are preferred. Free-space LEDs can be used to excite phosphors incorporated into the optical fibers (Scheme 1c). However, the efficiency of such excitation is limited. A better approach is to use FC-LCs excited by free-space LEDs, where the QD phosphors are incorporated within the polymer matrix of the LC (Scheme 1d) instead of in optical fibers. In this case, efficient and cheap excitation can be achieved. Furthermore, it is possible to utilize several independently excited and differently colored FC-LCs and combine the broadband spectrum in a spliced output optical fiber. By adjusting the excitation power of individual FC-LCs, a widely tunable output spectrum can be achieved in a single device. Even more, using different excitation wavelengths for each of the FC-LC allows for better coverage of the 400−500 nm spectral range. For example, the same type of LEDs with wavelengths ranging from 365 to 410 nm in increment of 5 nm are readily available. Several other

DOI: 10.1021/acsnano.9b03335
ACS Nano XXXX, XXX, XXX−XXX

wavelengths, such as 425, 440, 450, and 490 nm, are also implemented for the same LEDs. This can also be helpful for efficient excitation of the QDs emitting at 550 nm (see below).

While LCs are typically designed to have a large size, absorb a certain portion of sunlight, and deliver the re-emitted light to solar cells attached to the sides of the LC, there are alternative designs that could be used for other applications. In our devices, the FC-LC can effectively absorb all of the excitation light from an LED, couple it to an attached optical fiber, and guide the emitted light to an output. In this instance, the size of the FC-LC is not dictated by an external parameter, such as window size, but instead can be treated as an optimization parameter to achieve maximum coupling efficiency to the optical fiber. Likewise, FC-LC absorption can be optimized to efficiently convert all of the excitation light into a target emission without introducing any excess losses due to scattering. Moreover, escape cone losses can be diminished by applying reflective coatings on the side opposite to the excitation of the FC-LC. Coating the edges of the FC-LC with a reflective material can also be beneficial for device performance.

$CuInSe_xS_{2-x}$/ZnS QDs represent an ideal, inexpensive, low-hazard material for use as phosphors in FC-LCs. Figure 1a shows that QD emission can be tuned across most of the visible and NIR spectral regions by changing the size and composition of the nanocrystals. Moreover, emission from each of the QD sizes/compositions is broadband, so that the required spectral range, 400−1600 nm, can be covered by QDs emitting only at few selected wavelengths. Altogether, these properties enable the design of an efficient, broadband, fiber-coupled light source. Fully optimized QDs from UbiQD exhibit QYs over 95% across most of the tunable spectral range (590−1100 nm), while somewhat lower QYs (∼75%) have been achieved at the edges of the tunability range (550 nm and 1100−1250 nm). When the ZnS shell is grown on $CuInSe_xS_{2-x}$ QDs, alloying at the core/shell interface (due to small lattice mismatch between ZnS and $CuInSe_xS_{2-x}$) leads to blue-shift of the emission from original core wavelength. The observed blue-shift is usually largest for the $CuInSe_xS_{2-x}$/ZnS QDs emitting at ∼1250 nm due to introduction of both Zn and S atoms into the QD's core. For the 550 nm QDs, standard ZnS shell synthesis procedure leads to not only alloying but also to the creation of antisite and substitutional defects, which may affect the brightness of the QDs. Further optimization of ZnS shell growth procedure to improve quantum yield of the QDs emitting at longer and shorter wavelengths is underway, and the results will be reported elsewhere. Figure 1b shows that a broadband spectrum covering 440−1400 nm can be realized by combining QDs emitting at 650, 780, 990, and 1150 nm in a polymer slab with their concentrations adjusted to compensate for the size/composition-dependent difference in absorption cross-sections at the excitation wavelength (450 nm).

With emission bandwidths of ∼120 nm, these QDs were judiciously selected so that the spacing between the PL peaks would be close to an optimal value of ∼100−140 nm. In order to cover a broader spectral range, 500−1600 nm, two more QDs would be required with the peak positions close to 550 and 1250 nm. However, 405 nm or even shorter wavelength excitation is required for the 550 nm QDs, while further optimization is still ongoing to achieve ∼95% QY for the 1250 nm QDs. In order to simplify our prototypes, here we limit our discussion to the spectral range of 600−1400 nm.

In order to manufacture high-performance FC-LC prototypes, we optimized the LC form-factor (shape and size), fiber type, QD concentration, and fiber attachment method. Tested FC-LCs were made by incorporating QDs into a liquid monomer resin. The resin was cured under UV light in a mold formed from a rubber gasket sandwiched between glass. Part of the mold included an opening for a glass optical fiber (Thorlabs FP1000ERT) that was inserted into the mold after injection of the liquid resin. The width, length and thickness of the active area was determined by the gasket shape and size. The fabricated samples were excited using a 50 mW blue LED (450 nm). Figure S1 summarizes some of the configurations that were tested and their respective output powers for FC-LCs with fixed QD concentration. Square LCs (1 cm^2 active area) were found to be more efficient compared to LCs with an elongated form factor. We also observed better performance by coupling the optical fiber to the bulk of the LC, rather than to its edge or top surface. Further, by coating one of the sides of the LC and its edges with a reflective paint, we were able to effectively reduce escape cone losses and increase absorption of excitation while maintaining low reabsorption and high LC clarity. QD concentrations between 1 wt % (for elongated devices) and 4 wt % (for square devices after additional optimization in resin formulation to improve clarity) were found to be best for efficient absorption of excitation in a high clarity LC device.

A first prototype of the FC-LC was manufactured based on the optimized device design parameters explored. To optically characterize the device, a Thorlabs BFT1 adapter was used to terminate the FC-LC with a standard SMA905 connector. Photos in Figure 2a show red PL emission of the FC-LC

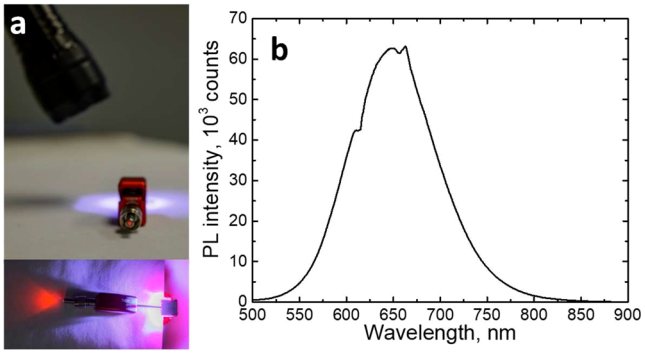

Figure 2. (a) Photos of the FC-LS excited by blue LED flashlight (top) and ChanZon blue LED (bottom). (b) PL spectrum (uncorrected for spectral response of the spectrometer) shows FC-LC output measured using fiber-coupled spectrometer.

prototype upon excitation with a blue LED flashlight and miniature blue LED (ChanZon 10DGL-DZ-3W-BL). Figure 2b presents the PL spectrum of the prototype when excited by the miniature blue LED. In order to characterize the broadband spectrum, the fiber was connected to an Avantes 2048USB2 spectrometer and the spectrum was collected using a 1.5 ms integration time. An output efficiency of 0.2% was measured for the first complete FC-LC prototype. While this value was lower than expected, it was encouraging because we could still measure a strong signal even at the spectrometer's shortest integration time (1 ms). Moreover, as FC-LCs do not emit much heat, the complete broadband light source should still be more efficient than the fiber-coupled tungsten halogen

DOI: 10.1021/acsnano.9b03335
ACS Nano XXXX, XXX, XXX−XXX

lamp. Further optimization of the device is expected to improve the output brightness (see below) enough for practical applications. The complete FC-LC package has a relatively small footprint of only 14 cm^3. The majority of the volume (10 cm^3) is occupied by a Thorlabs BFT1 adapter and the LC plus LED package has a footpring of just 1 cm^3. For comparison, a typical fiber-coupled tungsten halogen broadband light source, currently used for STS (Ocean Optics HL-2000-HP-FHSA), has a 10× footprint of ∼100 cm^3.

While a device output efficiency below 1% might suggest the need for further optimization, there exists a theoretical upper limit to this efficiency. Using equations presented in refs 5 and 6, one can estimate the total optical efficiency of the small LC (neglecting reabsorption/scattering losses) as $\eta_{opt} = QY(1 - R)A\eta_{trap}$, where QY is the quantum yield of the LC, R is the reflection coefficient of the LC, A is the absorption of the excitation light, and η_{trap} is the efficiency of light trapping into waveguide modes. Assuming a typical set of parameters, η_{trap} = 0.75 (based on escape cone losses between air and typical polymer or glass interface), R = 0.04 (typical reflection off the polymer or glass surface), QY = 0.95 (QY achieved for UbiQD's QDs), and A = 0.9 (based on the QD concentration and excitation wavelength), one can estimate the maximum attainable optical efficiency $\eta_{opt}^{max} \approx 0.62$. For the FC-LC without a reflective coating, the output efficiency can be estimated as $\eta = \eta_{opt}A_{fiber}/A_{edge}$, where A_{fiber} and A_{edge} are fiber cross-sectional and edge areas, respectively. For our prototypes, typical values for these parameters were A_{fiber} = 0.785 mm^2 and A_{edge} = 40 mm^2, so that the maximum coupling efficiency is expected to be $\eta^{max} \approx 1.2\%$. This value is somewhat higher compared to the experimentally realized efficiency, indicating that further improvements can be made to the device design.

In order to demonstrate the use of FC-LCs as a broadband light source, UbiQD manufactured several prototype FC-LCs using different sizes and compositions of the $CuInSe_xS_{2-x}/ZnS$ QDs. Three different prototypes with PL peak wavelengths of 590, 650, and 800 nm were tested (see Figure 3). Larger size

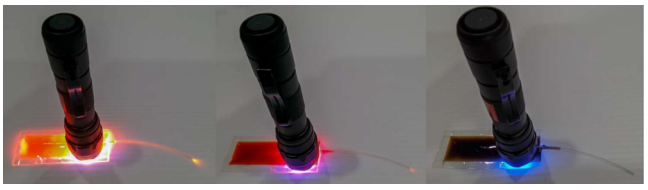

Figure 3. Photographs of three different FC-LCs with peak emission at 590, 650, and 800 nm excited by a blue LED flashlight. Output light is clearly observed for the FC-LCs with visible PL peaks.

(4 cm × 9 cm LC area) FC-LCs compared to the first version (1 cm × 1 cm LC area) were manufactured to simplify the handling and processing of the prototypes. This also improved photostability of the devices as barrier film was used to protect them from oxygen ingress. Namely, the devices were photostable under illumination (60 mW/cm^2, which is close to the typical excitation conditions) for more than 2000 h, as illustrated in Figure S2. An output power as high as 0.7 mW with the efficiency up to 0.8% was achieved without the use of a reflective coating. The improved efficiency was, most likely, achieved due to simplified manufacturing process, as well as better photostability.

In the next step, it was demonstrated that the FC-LC prototypes could be used in biological applications even before the final broadband light source is assembled. To do so, a simple test was performed using a single-color FC-LC. In STS applications, the absorption features of biologically relevant species, such as oxy- and deoxy-hemoglobin, water, and lipids, are measured since they have distinct absorption peaks in the visible and NIR spectral range, as shown in Figure 4a. By analyzing these absorption features, information on intrinsic physiological tissue properties can be obtained and then used to diagnose cancer, or other diseases.

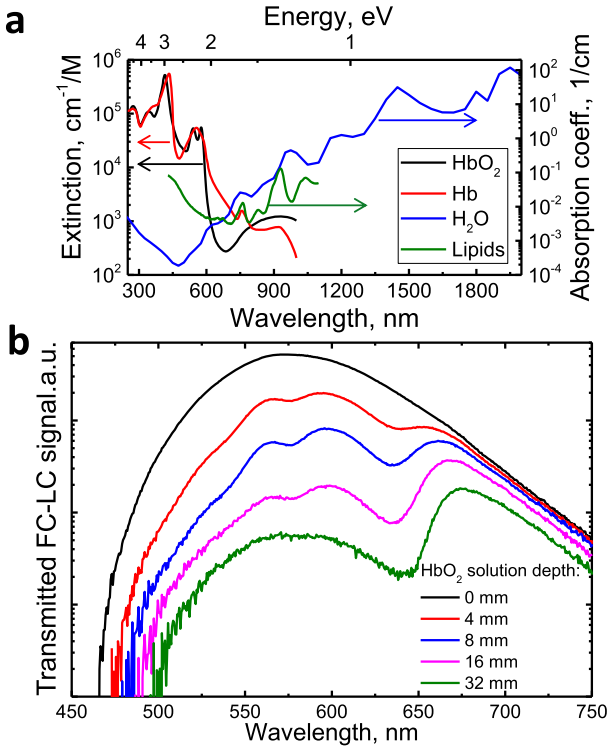

Figure 4. (a) Absorption spectra of the species relevant in determining intrinsic physiological tissue properties (oxy- and deoxyhemoglobin, water, and lipids) exhibit distinct peaks in the visible and NIR spectral range. (b) FC-LC with PL peak at 590 nm is used to monitor changes in concentration (or depth at constant concentration, as it is easier to realize in a demonstration experiment) of a hemoglobin solution.

To test the FC-LCs, we used a simplified biological sample, containing oxygenated hemoglobin (HbO_2) with distinct absorption features near 540 and 576 nm, and water or phosphate-buffered saline solution (PBS) with a weak absorption peak at ∼625 nm. To simulate measuring different concentrations of HbO_2 in the PBS, we used the FC-LC to measure different volumes of the biological sample. Measurements of the emission from the FC-LC passing through the vial containing HbO_2 in PBS buffer solution with increasing depth (amount of solution in the vial) are shown in Figure 4b. The depth was varied from 0 to 4, 8, 16, and 32 mm by adding more solution into the vial. At depths up to 16 mm, HbO_2 was clearly identified by all absorption peaks clearly discerned as dips (local minima) in the PL spectra. While changes in absorption of up to 2 orders of magnitude can be easily detected, HbO_2 cannot be readily identified at the largest depth (32 mm) because the PBS buffer absorption dominates

DOI: 10.1021/acsnano.9b03335
ACS Nano XXXX, XXX, XXX−XXX

the signal. This saturation behavior is observed at an optical density of ∼2, which is similar to behavior in typical detection devices.

In order to prove that the theoretical maximum coupling efficiency can be achieved, a champion FC-LC was manufactured by combining optimal design features gathered from the prototypes described above, with a reflective coating included. An output efficiency of 1.1% was measured for the champion device. Furthermore, the acquisition time needed to saturate the fiber-coupled spectrometer with this device would be as short as ∼0.3 ms, which is below the typical hardware limits. Despite the possible reduction of the signal in real-world STS applications, the measured signal should still be enough to operate close to the fastest spectrometer speed, which is important for rastering the tissues during STS measurements. This is comparable to what can be achieved using a typical tungsten halogen lamps. Therefore, FC-LCs have promise as alternative broadband light sources for STS as they offer smaller footprint and reduced cost compared to the traditional tungsten halogen lamps, all while maintaining a similar level of brightness.

Agricultural FC-LCs for Lower Canopy Lighting. The amount of sunlight and its spectrum are two important determining factors in the rate of plant growth. In greenhouse horticulture, the growth of vine plants such as tomatoes or cucumbers is limited by the amount of light that can be absorbed by the upper leaves of the plants. Typically, the upper leaves become saturated at high light levels and cannot produce more biomass if the light intensity is further increased. The lower leaves, however, are typically shaded by the upper canopy; thus, plant production can be increased if more light is directed to the lower canopy. Therefore, a device similar to the FC-LC broadband light source described above can be implemented in commercial agriculture. For this application, a QD-embedded nanocomposite would absorb light above the plant canopy and down-convert it. The emitted light can then be coupled into fiber optics and guided to the lower canopy. These devices employ $CuInS_2$/ZnS QDs emitting at 600 nm, which matches the wavelengths of light that are most efficient for photosynthesis.[21,22] In contrast to the broadband light source described above, the prototype FC-LC for agriculture combines multiple LCs into long bundles of acrylic optical fibers. The major differences between the FC-LCs discussed above and the devices described in this section are the length and number of optical fibers being coupled to the LC. In our agricultural devices, a multitude of longer fibers are attached to each collector in order to increase the light power delivered to the plants.

In order to maximize the amount of light delivered to the plants, several parameters, including the size of the LCs, the QD concentration, the number of fibers attached per LC, and the number of collector segments per device were optimized. During the optimization process, the samples were excited using a large-area blue LED at a flux of 1.51 mW/cm^2, and the output power from the fibers was measured using a Si power meter. The optimization procedure showed that the LCs with an active area of 24 cm^2 gave the highest output power. Additionally, the number of fibers attached per LC was varied between 1 and 6 (mainly limited by the size of LC edge), and the optimum output power was achieved for a device with five optical fibers. QD concentration was also optimized in order to reach a balance between maximal sunlight collection, minimal PL reabsorption, and high clarity in the LC waveguiding material. Finally, it was found that to achieve the desired total output power per plant, four of the individual FC-LCs needed to be combined in a single device, which provided sufficient light output while still being small enough not to disrupt airflow within a greenhouse.

After optimizing the device parameters, multiple prototype FC-LC devices consisting of four collectors (3 cm × 8 cm each) with five 4 ft-long fibers per collector were manufactured and characterized (Figure 5a). Using the large-area blue excitation source, the power output of the devices was measured to be 0.37 mW/cm^2, with a conversion efficiency of 24.5%. We also characterized the devices in the sun as to compare the PAR output from the fibers to the PPF from the incident sunlight. The measurements were done at noon on a clear sunny day. The PPF of the sun measured with a portable spectrometer was 1340 μmol m^{-2} s^{-1}. The FC-LC device was then oriented horizontally, and the output of the fibers was shaded (to minimize effect of the background sunlight). The measurement using the same spectrometer yielded 154 μmol m^{-2} s^{-1}. Therefore, since the lower canopy only receives ∼10% the amount of PAR as the upper canopy, our fiber devices could potentially double the amount of light the lower canopy leaves could absorb.

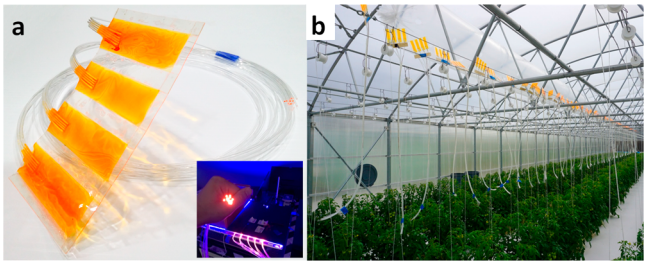

Figure 5. (a) Photographs of the prototyped FC-LC for agriculture. Inset shows emission from the agriculture FC-LC under a large-area blue LED excitation. (b) 82 collectors deployed over a row of tomatoes in a commertial hydroponic greenhouse.

Once a desired prototype was successfully designed, manufactured, and characterized, we proceeded to fabricate and assemble more than 80 devices to be installed in a commercial hydroponic tomato greenhouse owned by Growing Opportunities, Inc., and located in northern New Mexico. As this was the first trial to show the feasibility of using FC-LCs for agriculture application in a commercial greenhouse, no penetrations made in the greenhouse were allowed to position FC-LCs outside, so the devices were placed inside the greenhouse above the tested plants. Figure 5b shows a photograph of the LC devices after installation in a commercial greenhouse.

For this trial, we investigated the growth behavior of two different rows of beefsteak tomatoes in the same greenhouse (180 plants each), where 82 FC-LC devices were deployed on only a portion of one row to provide coverage for 92 plants. The plant rows were within the same commercial greenhouse, close to each other in location, and were subject to the same environmental controls to ensure they had similar environments, including temperature, humidity and light levels. The trial was conducted over a 6-month period (June−December 2018), out of which for the first month no crop was harvested as the plants were developing. By the grower's standard procedure, the tomatoes were harvested twice a week and the

DOI: 10.1021/acsnano.9b03335
ACS Nano XXXX, XXX, XXX−XXX

total fresh weight yields per row were recorded from both the test and control rows.

At the conclusion of the tomato trial, the cultivator reported back a 7% improvement (compared to the control) in weight yield from the row that utilized the FC-LCs, as summarized in Figure 6. The benefit was the largest in the first month of harvest, but it was not observed during the second month of the harvest. For the next three months, however, the benefit continued to increase, such that by the end of study, the plants grown with the help of FC-LCs produced almost two hundred additional pounds of tomatoes. This translates to an increase of the crop by ∼2 pounds per plant.

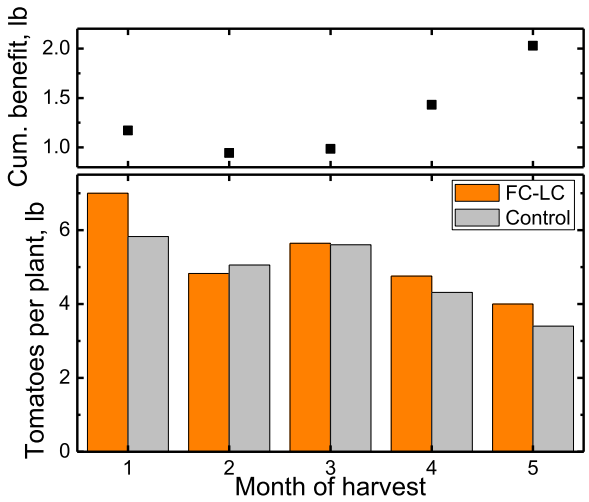

Figure 6. Comparison of the tomato crop yield with and without use of FC-LCs highlights the benefits of the FC-LCs: a 7% increase in crop yield per plant is observed when FC-LCs are used compared to the control, which has no devices. Top graph shows cumulative benefit weight of crop per plant when using FC-LCs compared to the control. Bottom section directly compares the total harvested weight (per plant) each month from the plants grown with and without FC-LCs. For simplicity, the data are bundled into harvest per month.

One might ask how decreasing of the light level above the plants from absorption and redirection of light by the LC might impact the overall growth benefit. Typically, under low light conditions, there is a rule that 1% more PAR results in 0.5−1% crop yield improvement.[26] The yield improvement due to light intensity depends on the type of plant, season, temperature, and other growth factors, but in this low light regime leaves are not saturated by light and can continue to increase production almost linearly. However, once the light intensity increases to a certain level, the net photosynthetic rate of the plant (defined as the difference between the total amount of photosynthesis and the total rate of respiration) will eventually saturate. Before complete light saturation, the net photosynthetic rate of the plant will start leveling off and the amount of yield benefit due to higher light levels will be less. According to Masabni *et al.*,[27] in the case of tomatoes, light levels up to about 1000 μmol m^{-2} s^{-1} result in significant changes in the net photosynthetic rate, but after that point, increases in the net photosynthetic rate are minor until saturated at 2000 μmol m^{-2} s^{-1}. Therefore, during the grow season when light levels are high (*e.g.*, > 1000 μmol m^{-2} s^{-1}) it can be beneficial for the plant to reduce the light levels at the upper canopy in order to provide more light to the lower leaves. This is what was observed in the tomato trial.

Luminescent Detectors for Telecommunication. Strong absorption and near-unity QYs of $CuInSe_xS_{2-x}$/ZnS QDs make them an attractive active material for luminescent detectors. Consequently, an FC-LC design similar to those suitable for biomedical and agricultural applications can also be used to improve free-space telecommunication systems.

As a first step of the LC-based receiver demonstration, two FC-LCs (with 590 and 800 nm PL peaks) were tested in order to validate the technology. The FC-LCs were excited using modulated laser or LED light, and the fiber output was coupled to a Si photodiode detector. The detector's output voltage was sent to either a fast digital oscilloscope or to a lock-in amplifier. Due to limitations of the photodiode detector and excitation sources available in our lab, only 1 kHz modulation was used in these experiments. Excitation wavelengths of 450 and 640 nm were used. Given the large Stokes shift (∼350−450 meV)[4] in $CuInSe_xS_{2-x}$/ZnS QDs, the 450 nm excitation would be expected to efficiently excite both FC-LCs, while the 640 nm wavelength would only efficiently excite the 800 nm FC-LC and should be weakly coupled into the 590 nm FC-LC. This weak coupling is a consequence of the fact that a small amount of excitation light is scattered on the imperfections of FC-LC and trapped inside by total internal reflection. It is then coupled to the optical fiber, the same way as the regular PL.

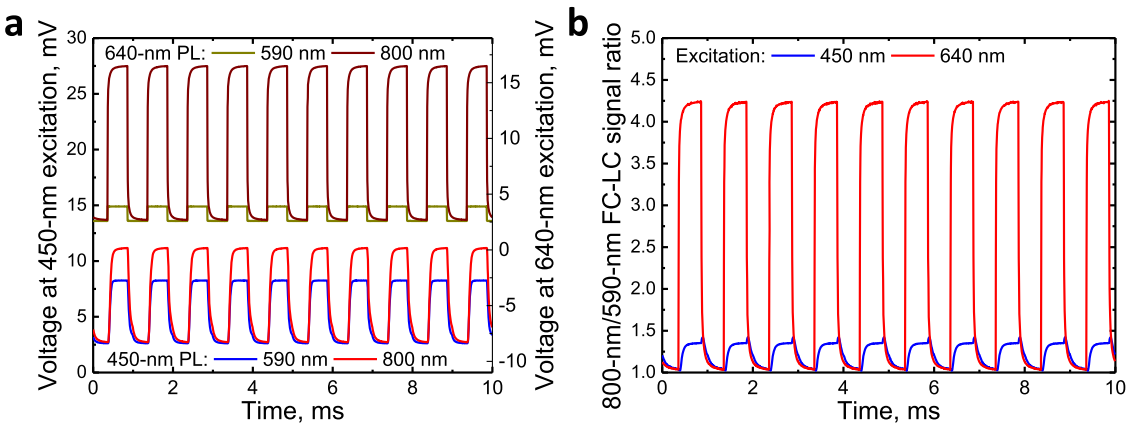

Figure 7. (a) Excitation of the 590 and 800 nm FC-LCs by 450 and 640 nm light result in a clear signal on the Si photodiode. (b) Ratio of the signals from the two FC-LCs is drastically different for the 450 and 640 nm excitations, allowing for color differentiation.

DOI: 10.1021/acsnano.9b03335
ACS Nano XXXX, XXX, XXX−XXX

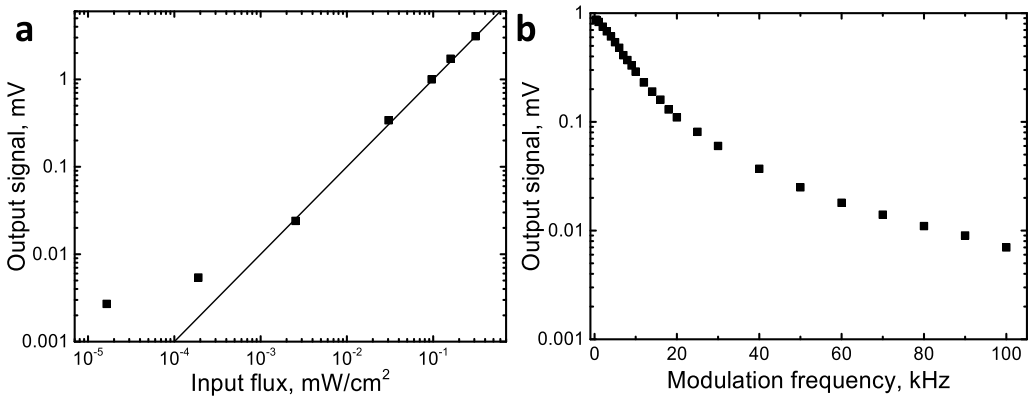

Figure 8. (a) Using lock-in detection, linearity (black solid line) of the FC-LC+photodiode system is observed with excitation flux as low as ~10^{-3} mW/cm^2. (b) Modulation frequencies up to 100 kHz are demonstrated, although it is expected that much faster speed is possible using faster photodiode and excitation source.

The average flux of the two excitation sources was measured at 0.3 and 4 mW/cm^2 for the 450 and 640 nm excitation wavelengths, respectively. Figure 7a shows the response of a Si photodiode coupled to the FC-LCs under the above-mentioned excitations. Upon 450 nm excitation (bottom blue/red curves), both FC-LCs show comparable responses, while the 640 nm excitation (top dark yellow/wine curves) results in a much stronger signal for the 800 nm FC-LC compared to that of the 590 nm device. This is due to the fact that only the 800 nm QDs can be directly excited by 640 nm. Moreover, the shape of the signal from the 640 nm excited 590 nm FC-LC is somewhat different from the other signals, and more closely resembles the excitation light than it does the PL of the QDs because some fraction of the excitation light is coupled into the Si photodiode detector through the optical fiber of the FC-LC. Additionally, we observe that the signal is always above zero, even when the excitation is off. This can be attributed to a constant background caused by the excitation of the LCs by ambient light. The ratio of the signals from two FC-LCs with excitation at 450 and 640 nm is shown in Figure 7b. The ratio is below 1.5 and above 4.0 during the 450 and 640 nm excitation, respectively. The ratio is close to 1.0 when the excitation is off. A greater than 2-fold difference in these ratios makes them easy to discern. Moreover, the shape of the ratios differs between the two excitations. Therefore, collecting the signal simultaneously using several FC-LCs with different peak PL wavelengths, can enable schemes with color detection.

Further, to test the excitation power limit, we used both FC-LCs to measure signals occurring after the 450 nm excitation attenuated using a neutral density filter with an optical density of 1. The responses of both FC-LCs to this excitation are shown in Figure S3. A linear dependence of the device response on the excitation flux is observed. Additionally, a clear modulated signal is still observed at such a low excitation flux.

Further attenuation of the excitation is still possible, especially when lock-in detection is used. Figure 8a shows that the linearity of the detection system is preserved down to an excitation flux of ~10^{-3} mW/cm^2 when a 20 dB gain setting is used on the photodiode. This is 2 orders of magnitude better than that reported in ref 25. Figure 8b shows that using a 0 dB gain setting allows for faster modulation frequency, although limitations of the experimental setup do not allow data speeds of more than 100 kHz. In principle, a modulation frequency of up to 530 kHz should be easily achievable given the QD's PL lifetimes of ~300 ns ($f_{-3DB} = 1/(2\pi\tau)$,[25] where τ is the PL lifetime). Here, we stress again that the use of FC-LCs as luminescent detectors is to split the detection scheme into two parts—one (fast small area photodiode) for the fast detection by conversion of photons into electrons, and the other (larger-area FC-LC) for all-optical collection of the optical signals transmitted through the atmosphere using much larger detection area (up to 3 orders of magnitude), such that the detection is insensitive to pointing instability of the free-space telecommunication system. Even faster frequencies can be achieved if the radiative lifetime can be shortened. An attractive strategy to achieve this involves the introduction of metal plasmonic structures into the FC-LSs.[28] More complex core/shell nanocrescents, similar to those described in ref 29, can be synthesized around each QD to shorten PL lifetime up to 40-fold. As a result, modulation frequencies above 20 MHz are possible. Further reduction of the PL lifetimes through the control of the local dielectric environment and QD-plasmonic structures synthesis is required to achieve even faster modulation.

CONCLUSIONS

In conclusion, we have demonstrated prototypes of FC-LCs for applications as broadband light sources for biomedical diagnostics, waveguiding sunlight collectors for agriculture, and large-area luminescent detectors for free-space telecommunication. Each device was built upon the same core fiber-coupled QD-based technology but underwent different optimization steps in order to meet the needs of its respective application.

Cancer is the leading cause of death, and so any improvements in our ability to diagnose cancer earlier will have significant impacts. FC-LCs have promise as alternative broadband light sources for STS in cancer diagnostics as they offer a smaller footprint and reduced cost compared to the traditional tungsten halogen lamps, all while maintaining a similar level of brightness.

An emerging global problem is the long-term decreasing amount of agricultural land per capita. The trends of increasing population, urbanization, diminishing water supply, and continuing climate change have contributed to declining stocks of arable land per person. Almost every aspect of greenhouse agriculture is fully optimized and controlled precisely, from the nutrient delivery system and irrigation to the temperature and CO_2 levels, but the quantity and quality of sunlight varies by season and climate. There currently is

DOI: 10.1021/acsnano.9b03335
ACS Nano XXXX, XXX, XXX−XXX

minimal effort put into controlling the light spectrum in the greenhouse where growers mainly depend on the sun's spectrum for growing crops, which varies by season and climate. Today, the only way to control spectrum in a greenhouse is with expensive lighting that consumes electricity. Using FC-LCs to provide optimized spectra to the lower canopy of plants could be a sustainable, low-cost route to improve crop yields for greenhouse growers.

Free-space telecommunication is ubiquitous, and most can appreciate the value of improving signal-to-noise ratios in such systems. We have shown that large-area luminescent detectors can be used to discern time-modulated unfocused signals with an average power as low as 1 μW, which could have a significant impact in applications like autonomous vehicles and LiFi.

Future development and optimization will be needed for the commercialization of FC-LCs, but the proofs-of-concept shown in this work will hopefully inspire others to work on FC-LC applications. It is unusual that a technology can have such a breadth of uses as FC-LCs, and perhaps medical diagnostics, plants growth enhancement, and free-space telecommunication systems are just the beginning.

METHODS

Optical characterization of the QDs and FC-LCs was performed using commercial absorption (Carry-8454) and emission (Horiba FluoroMax-4) spectrometers and a home-built NIR emission spectrometer equipped with an InGaAs photodiode detector (Thorlabs PDF10C) and a lock-in amplifier (Stanford Research Systems SR830 DSP). A Thorlabs PM100USB power meter and a S120VC Si head were used to measure the input power of the excitation LEDs, laser, and output power of the FC-LCs. A Si photodiode detector (Thorlabs PDA36A) connected to a fast oscilloscope (Agilent Technologies DSO-X 3032A) was used to measure the response of the FC-LC-based receivers. A fiber-coupled spectrometer (Avantes 2048USB2) was used to measure the spectra of the FC-LCs. Excitation sources included blue LEDs (Thorlabs M455F1 and ChanZon 10DGL-DZ-3W-BL), as well as a 640 nm laser (Coherent Cube).

$CuInSe_xS_{2-x}$/ZnS QDs were synthesized using methods similar to those described in ref 30 with minor modifications aimed to maximize PL QY and scale up the synthesis. QDs emitting at wavelengths between 550 and 900 nm are $CuInS_2$/ZnS with size varying from 3 to 9 nm with a typical size distribution of ∼15−19%. QDs emitting between 950 and 1250 nm are $CuInSe_xS_{2-x}$/ZnS (x = 0.25−1.75) with size varying from 5 to 10 nm with a typical size distribution of ∼12−16%. Both sulfide and mixed sulfide/selenide QDs have tetrahedral shape. Transmission electron images of representative QDs emitting at 590 and 990 nm are shown in Figure S4. FC-LCs were manufactured in several steps. First, three-sided pockets of a predefined size were made from PET film and a double-sided tape to prevent resin leakage. The optical fiber(s) were then incorporated into the unsealed side of the pocket and fixed into position using more tape. Next, an acrylate QD resin described in ref 5 was injected into the empty pocket from the unsealed side and cured under UV illumination. The resin was formulated to have appropriate viscosity and good adhesion to PET and contain up to 4 wt % of $CuInSe_xS_{2-x}$/ZnS QDs. Several postprocessing steps were run after resin curing, including cleaning of the fibers, packaging of the fibers for easier use and installation, and the application of a reflective coating.

ASSOCIATED CONTENT

Supporting Information

The Supporting Information is available free of charge on the ACS Publications website at DOI: 10.1021/acsnano.9b03335.

Comparison of characteristics for various materials, design optimization of FC-LCs, photostability of FC-LCs, and low-excitation power FC-LCs modulation signal (PDF)

AUTHOR INFORMATION

Corresponding Author

*E-mail: nikolay@ubiqd.com. Tel: 505-310-6766.

ORCID

Nikolay S. Makarov: 0000-0003-1041-0401

Hunter McDaniel: 0000-0002-5009-918X

Notes

The authors declare no competing financial interest.

ACKNOWLEDGMENTS

This work was performed, in part, at the Center for Integrated Nanotechnologies, an Office of Science User Facility operated for the U.S. Department of Energy (DOE) Office of Science by Los Alamos National Laboratory (Contract DE-AC52-06NA25396) and Sandia National Laboratories (Contract DE-NA-0003525). We acknowledge Steve and Kim Martin of Growing Opportunities, Inc., for use of their greenhouse facilities and for harvesting the tomatoes in the plant trial of this paper.

REFERENCES

(1) Weber, W. H.; Lambe, J. Luminescent Greenhouse Collector for Solar Radiation. *Appl. Opt.* **1976**, *15*, 2299−2300.

(2) Goetzberger, A.; Greube, W. Solar Energy Conversion with Fluorescent Collectors. *Appl. Phys.* **1977**, *14*, 123−139.

(3) Bomm, J.; Büchtemann, A.; Chatten, A. J.; Bose, R.; Farrell, D. J.; Chan, N. L. A.; Xiao, Y.; Slooff, L. H.; Meyer, T.; Meyer, A.; van Sark, W.G.J.H.M.; Koole, R. Fabrication and Full Characterization of State-of-the-Art Quantum Dot Luminescent Solar Concentrators. *Sol. Energy Mater. Sol. Cells* **2011**, *95*, 2087−2094.

(4) Meinardi, F.; McDaniel, H.; Carulli, F.; Colombo, A.; Velizhanin, K. A.; Makarov, N. S.; Simonutti, R.; Klimov, V. I.; Brovelli, S. Highly Efficient Large-Area Colourless Luminescent Solar Concentrators Using Heavy-Metal-Free Colloidal Quantum Dots. *Nat. Nanotechnol.* **2015**, *10*, 878−885.

(5) Bergren, M. R.; Makarov, N. S.; Ramasamy, K.; Jackson, A.; Guglielmetti, R.; McDaniel, H. High-Performance $CuInS_2$ Quantum Dot Laminated Glass Luminescent Solar Concentrators for Windows. *ACS Energy Lett.* **2018**, *3*, 520−525.

(6) Klimov, V. I.; Baker, T. A.; Lim, J.; Velizhanin, K. A.; McDaniel, H. Quality Factor of Luminescent Solar Concentrators and Practical Concentration Limits Attainable with Semiconductor Quantum Dots. *ACS Photonics* **2016**, *3*, 1138−1148.

(7) American Cancer Society. *Cancer Facts & Figures 2017*, https://www.cancer.org/content/dam/cancer-org/research/cancer-facts-and-statistics/annual-cancer-facts-and-figures/2017/cancer-facts-and-figures-2017.pdf; American Cancer Society: Atlanta; 2017 (accessed Apr 10 2019).

(8) Etzioni, R.; Urban, N.; Ramsey, S.; McIntosh, M.; Schwartz, S.; Reid, B.; Radich, J.; Anderson, G.; Hartwell, L. The Case for Early Detection. *Nat. Rev. Cancer* **2003**, *3*, 1−10.

(9) Bard, M. P.; Amelink, A.; Hegt, V. N.; Graveland, W. J.; Sterenborg, H. J. C. M.; Hoogsteden, H. C.; Aerts, J. G. J. V. Measurement of Hypoxia-Related Parameters in Bronchial Mucosa by Use of Optical Spectroscopy. *Am. J. Respir. Crit. Care Med.* **2005**, *171*, 1178−1184.

(10) Volynskaya, Z.; Haka, A. S.; Bechtel, K. L.; Fitzmaurice, M.; Shenk, R.; Wang, N.; Nazemi, J.; Dasari, R. R.; Feld, M. S. Diagnosing Breast Cancer Using Diffuse Reflectance Spectroscopy and Intrinsic Fluorescence Spectroscopy. *J. Biomed. Opt.* **2008**, *13*, No. 024012.

(11) Cerussi, A. E.; Shah, N.; Hsiang, D.; Durkin, A.; Butler, J.; Tromberg, B. J. *In Vivo* Absorption, Scattering, and Physiologic

DOI: 10.1021/acsnano.9b03335
ACS Nano XXXX, XXX, XXX−XXX

Properties of 58 Malignant Breast Tumors Determined by Broadband Diffuse Optical Spectroscopy. *J. Biomed. Opt.* **2006**, *11*, No. 044005.
(12) Brown, J. Q.; Wilke, L. G.; Geradts, J.; Kennedy, S. A.; Palmer, G. M.; Ramanujam, N. Quantitative Optical Spectroscopy: A Robust Tool for Direct Measurement of Breast Cancer Vascular Oxygenation and Total Hemoglobin Content *In Vivo*. *Cancer Res.* **2009**, *69*, 2919−2926.
(13) Amelink, A.; Sterenborg, H. J. C. M.; Bard, M. P. L.; Burgers, S. A. *In Vivo* Measurement of the Local Optical Properties of Tissue by Use of Differential Path-Length Spectroscopy. *Opt. Lett.* **2004**, *29*, 1087−1089.
(14) Amelink, A.; van der Ploeg; van den Heuvel, A.; de Wolf, W. J.; Robinson, D. J.; Sterenborg, H. J. C. M. Monitoring PDT by Means of Superficial Reflectance Spectroscopy. *J. Photochem. Photobiol., B* **2005**, *79*, 243−251.
(15) Tran, W. T.; Gangeh, M. J.; Sannachi, L.; Chin, L.; Watkins, E.; Bruni, S. G.; Rastegar, R. F.; Curpen, B.; Trudeau, M.; Gandhi, S.; Yaffe, M.; Slodkowska, E.; Childs, C.; Sadeghi-Naini, A.; Czarnota, J. G. Predicting Breast Cancer Response to Neoadjuvant Chemotherapy Using Pretreatment Diffuse Optical Spectroscopic Texture Analysis. *Br. J. Cancer* **2017**, *116*, 1329−1339.
(16) Evers, D. J.; Nachabe, R.; Vranken Peeters, M. J.; van der Hage, J. A.; Oldenburg, H. S.; Rutgers, E. J.; Lucassen, G. W.; Hendriks, B. H.; Wesseling, J.; Ruers, T. J. Diffuse Reflectance Spectroscopy: Towards Clinical Application in Breast Cancer. *Breast Cancer Res. Treat.* **2013**, *137*, 155−165.
(17) Bigio, I. J.; Bown, S. G. Spectroscopic Sensing of Cancer and Cancer Therapy. *Cancer Biol. Ther.* **2004**, *3*, 259−267.
(18) Tran, W. T.; Childs, C.; Chin, L.; Slodkowska, E.; Sannachi, L.; Tadayyon, H.; Watkins, E.; Wong, S. L.; Curpen, B.; El Kaffas, A.; Al-Mahrouki, A.; Sadeghi-Naini, A.; Czarnota, G. J. Multiparametric Monitoring of Chemotherapy Treatment Response in Locally Advanced Breast Cancer Using Quantitative Ultrasound and Diffuse Optical Spectroscopy. *Oncotarget* **2016**, *7*, 19762−19780.
(19) Nachabé, R.; Hendriks, B. H. W.; van der Voort, M.; Desjardins, A. E.; Sterenborg, H. J. C. M. Estimation of Biological Chromophores using Diffuse Optical Spectroscopy: Benefit of Extending the UV-VIS Wavelength Range to Include 1000 to 1600 nm. *Opt. Expr.* **2010**, *18*, 1432−1442.
(20) Shibles, R. Terminology Pertaining to Photosynthesis. *Crop Sci.* **1976**, *16*, 437−438.
(21) McCree, K. J. The Action Spectrum, Absorptance and Quantum Yield of Photosynthesis in Crop Plants. *Agricult. and Forest Meteorology.* **1971**, *9*, 191−216.
(22) McCree, K. J. Test of Current Definitions of Photosynthetically Active Radiation Against Leaf Photosynthesis Data. *Agricult. and Forest Meteorology.* **1972**, *10*, 443−453.
(23) Cope, K. R.; Snowden, M. C.; Bugbee, B. Photobiological Interactions of Blue Light and Photosynthetic Photon Flux: Effects of Monochromatic and Broad-Spectrum Light Sources. *Photochem. Photobiol.* **2014**, *90*, 574−584.
(24) Snowden, M. C.; Cope, K. R.; Bugbee, B. Sensitivity of Seven Diverse Species to Blue and Green Light: Interactions with Photon Flux. *PLoS One* **2016**, *11*, No. 0163121.
(25) Peyronel, T.; Quirk, K. J.; Wang, S. C.; Tiecke, T. G. Luminescent Detector for Free-Space Optical Communication. *Optica* **2016**, *3*, 787−792.
(26) Hemming, S. Use of Natural and Artificial Light in Horticulture − Interaction of Plant and Technology. *Acta Hortic.* **2011**, 25−36.
(27) Masabni, J.; Sun, Y.; Niu, G.; Valle, P. D. Shade Effect on Growth and Productivity of Tomato and Chili Pepper. *HortTechnol.* **2016**, *26*, 344−350.
(28) Saboktakin, M.; Ye, X.; Oh, S. J.; Hong, S.-H.; Fafarman, A. T.; Chettiar, U. K.; Engheta, N.; Murray, C. B.; Kagan, C. R. Metal-Enhanced Upconversion Luminescence Tunable through Metal Nanoparticle-Nanophosphor Separation. *ACS Nano* **2012**, *6*, 8758−8766.
(29) Atre, A. C.; García-Etxarri, A.; Alaeian, H.; Dionne, J. A. Toward High-Efficiency Solar Upconversion with Plasmonic Nanostructures. *J. Opt.* **2012**, *14*, No. 024008.
(30) McDaniel, H.; Koposov, A. Y.; Draguta, S.; Makarov, N. S.; Pietryga, J. M.; Klimov, V. I. Simple yet Versatile Synthesis of $CuInSe_xS_{2-x}$ Quantum Dots for Sunlight Harvesting. *J. Phys. Chem. C* **2014**, *118*, 16987−16994.

DOI: 10.1021/acsnano.9b03335
ACS Nano XXXX, XXX, XXX−XXX